ADVANCES IN ATMOSPHERIC SCIENCES, VOL. 29, NO. 6, 2012, 1159–1173

Summer Persistence Barrier of Sea Surface Temperature Anomalies in the Central Western North Pacific

ZHAO Xia[1,2,3] (赵 霞), LI Jianping*[2] (李建平), and ZHANG Wenjun[4,2] (张文君)

[1] *Laboratory of Ocean Circulation and Waves, Institute of Oceanology, Chinese Academy of Sciences, Qingdao* 266071

[2] *National Key Laboratory of Numerical Modeling for Atmospheric Sciences and Geophysical Fluid Dynamics, Institute of Atmospheric Physics, Chinese Academy of Science, Beijing* 100029

[3] *State Key Laboratory of Tropical Oceanography, South China Sea Institute of Oceanology, Chinese Academy of Sciences, Guangzhou* 51030

[4] *Key Laboratory of Meteorological Disaster of Ministry of Education and College of Atmospheric Sciences, Nanjing University of Information Science and Technology, Nanjing* 210044

(Received 5 December 2011; revised 22 February 2012)

ABSTRACT

The persistence barrier of sea surface temperature anomalies (SSTAs) in the North Pacific was investigated and compared with the ENSO spring persistence barrier. The results show that SSTAs in the central western North Pacific (CWNP) have a persistence barrier in summer: the persistence of SSTAs in the CWNP shows a significant decline in summer regardless of the starting month. Mechanisms of the summer persistence barrier in the CWNP are different from those of the spring persistence barrier of SSTAs in the central and eastern equatorial Pacific. The phase locking of SSTAs to the annual cycle does not explain the CWNP summer persistence barrier.

Remote ENSO forcing has little linear influence on the CWNP summer persistence barrier, compared with local upper-ocean process and atmospheric forcing in the North Pacific. Starting in wintertime, SSTAs extend down to the deep winter mixed layer then become sequestered beneath the shallow summer mixed layer, which is decoupled from the surface layer. Thus, wintertime SSTAs do not persist through the following summer. Starting in summertime, persistence of summer SSTAs until autumn can be explained by the atmospheric forcing through a positive SSTAs–cloud/radiation feedback mechanism because the shallow summertime mixed layer is decoupled from the temperature anomalies at depth, then the following autumn–winter–spring, SSTAs persist. Thus, summer SSTAs in the CWNP have a long persistence, showing a significant decline in the following summer. In this way, SSTAs in the CWNP show a persistence barrier in summer regardless of the starting month.

Key words: SST anomalies, persistence barrier, oceanic mixed layer, atmospheric forcing, positive cloud feedback on SSTAs

Citation: Zhao, X., J. P. Li, and W. J. Zhang, 2012: Summer persistence barrier of sea surface temperature anomalies in the central western North Pacific. *Adv. Atmos. Sci.*, **29**(6), 1159–1173, doi: 10.1007/s00376-012-1253-2.

1. Introduction

The presence of the spring persistence barrier in ENSO is well known. It refers to the rapid decline of the persistence of the ENSO index (e.g., Niño-3 SST anomalies (SSTAs) and Southern Oscillation pressure differences) in April–June regardless of the starting month (Troup, 1965; Wright, 1979; Webster and Yang,

*Corresponding author: LI Jianping, ljp@lasg.iap.ac.cn

1992; Lau and Nath, 1996; Clarke and Gorder, 1999; Xue et al., 1994; Yu, 2005; Mu et al., 2007; Duan et al., 2009; Duan and Zhang, 2010). The cause of this spring persistence barrier has not yet been fully elucidated, and various hypotheses have been suggested. Wright (1979) indicated that it may be related to the sign change of atmosphere–ocean feedbacks from one season to another. Webster and Yang (1992) and Lau and Yang (1996) suggested that the ENSO spring persistence barrier may be related to the influence of the Asian monsoon. Torrence and Webster (1998) proposed the phase locking of ENSO to the annual cycle as the cause of the spring persistence barrier. In addition to the eastern equatorial Pacific, persistence barriers of SSTAs also exist in other regions, such as the autumn (October–November) persistence barrier in the South China Sea (SCS) and the vicinity of Indonesia (Chen et al., 2007; Zhao and Li, 2009), the winter persistence barrier in the southeastern tropical Indian Ocean (Wajsowicz, 2005) and in the northern tropical Atlantic (Ding and Li, 2011).

However, whether a persistence barrier of SSTAs exists in the North Pacific remains unclear. This topic merits attention because mid-latitude atmosphere–ocean interactions exert strong influences on seasonal climate anomalies (Davis, 1978; Frankignoul, 1985; Wallace et al., 1990; Lau and Nath, 1990; Kushnir and Lau, 1992). Although previous analyses of SSTAs persistence (Alexander and Deser, 1995; Zhang et al., 1998; Park et al., 2006; Ding and Li, 2009) include the North Pacific, the persistence barrier of SSTAs in the North Pacific has not yet been examined specifically. Research on this topic would contribute to a better understanding of seasonal variations in SSTAs persistence in the North Pacific, and it would enhance our ability to perform seasonal climate prediction as well. In this study, we reported a significant summer persistence barrier in the central western North Pacific (CWNP), in addition to the spring persistence barrier in the eastern equatorial Pacific (Fig. 1); this phenomenon has characteristics substantially different than those of the ENSO spring persistence barrier. We aimed to examine the possible causes of the CWNP summer persistence barrier.

On one hand, ENSO exerts a strong influence on global climate variability, including the North Pacific Ocean (e.g., Pan and Oort, 1990; Trenberth et al., 1998) via the atmosphere bridge (e.g., Lau and Nath, 1996). Because the persistence of ENSO varies with the season and because ENSO exhibits the spring persistence barrier, we investigated whether ENSO influences SSTAs persistence in the CWNP or causes the summer persistence barrier. On the other hand, many studies have derived the intrinsic mid-latitude atmosphere–ocean coupled mode in the North Pacific, which is separated from the ENSO-induced mid-latitude coupled pattern (Deser and Blackmon, 1995; Zhang et al., 1996, 1997; An and Wang, 2005). Moreover, local atmospheric forcing and upper ocean processes can have an important impact on SSTAs in the North Pacific. Wintertime SSTAs in the mid-latitude North Pacific are primarily generated through surface turbulent heat flux changes in association with large-scale atmospheric circulation anomalies (e.g., Cayan, 1992). Local processes within the upper ocean, such as the seasonal variation in the depth of the surface mixed layer, may also lead to SST variability (e.g., Alexander and Deser, 1995). Thermodynamic feedbacks between marine stratus clouds and SST may also enhance the persistence of mid-latitude SSTAs, especially in summer (e.g., Zhang et al., 1998). Therefore, it is necessary to study the influences of atmospheric forcing and local ocean dynamical processes on the CWNP summer persistence barrier. Moreover, we sought to determine whether the mechanism of the CWNP summer persistence barrier is different from that of the ENSO spring persistence barrier. Comparison of the two phenomena contributes to a better understanding of different seasonal variations in SSTAs persistence between the extratropical Pacific and the tropical Pacific, including the atmosphere–ocean interaction in the extratropics and the tropics.

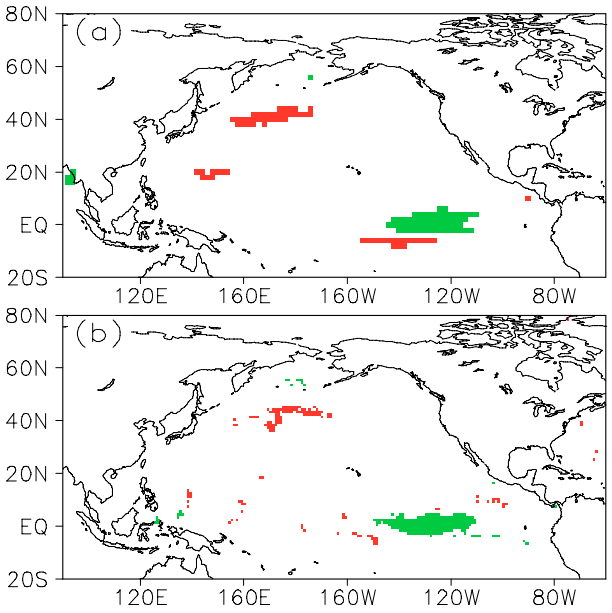

Fig. 1. Temporal–spatial distribution of the persistence barrier of SSTAs in the tropical and North Pacific, from (a) IERSST and (b) HADISST datasets. Green color indicates the barrier timing is spring; red color indicates the barrier timing is summer.

The remainder of this paper is organized as fol-

lows. The datasets and methodology are described in section 2, and the spatial–temporal characteristics of the persistence barrier of SSTAs in the tropical and North Pacific are presented in section 3. In section 4 we present a discussion of the causes of the summer persistence barrier of SSTAs in the North Pacific. Finally, a summary is provided in section 5.

2. Data and methodology

In this study, for an SST dataset we used the Improved Extended Reconstruction Sea Surface Temperature (IERSST, 2°×2° grid resolution) for 1950–2004 (Smith and Reynolds, 2004). The Hadley Centre Sea Ice and SST (HADISST) was used for confirming the spatial–temporal characteristics of the persistence barrier of SSTAs in the North Pacific (Rayner et al., 2003). Monthly subsurface temperature data were obtained from the Joint Environmental Data Analysis Center at the Scripps Institution of Oceanography (White, 1995). This archive contains temperatures at 11 levels (0 m, 20 m, 40 m, 60 m, 80 m, 120 m, 160 m, 200 m, 240 m, 300 m, and 400 m) during 1955–2003. The climatological monthly mean mixed layer depth (MLD) data were obtained from the *World Ocean Atlas 1994* (1°×1° grid resolution), where the MLD was determined as the depth at which the density difference from the sea surface is 0.125 sigma units (Monterey and Levitus, 1997). Atmospheric reanalysis data were obtained from the National Center for the Environmental Prediction–National Center for Atmospheric Research (NCEP–NCAR) for the period 1950–2004 (2.5°×2.5° grid resolution), including geopotential height and zonal wind (Kalnay et al., 1996). Monthly low cloud cover data were obtained from the European Center for Medium range Weather Forecasting (ECMWF) reanalysis for 1958–2001 (Uppala et al., 2005). The annual cycle of each variable was removed by subtracting the mean monthly value at each grid point.

According to previous definitions of the ENSO spring persistence barrier (Webster and Yang, 1992) and the SCS fall persistence barrier (Chen et al., 2007; Zhao and Li, 2009), we defined persistence in terms of lag correlation coefficients and the extent to which these coefficients remained at the 95% confidence level for lag times. Figure 2 shows the lag correlation coefficients of SSTAs in the Niño-3 SSTAs calculated with each respective starting month (January–December). The correlation curves were shifted to line up their 1-month lag with the calendar month shown on the abscissa. A persistence barrier is manifested as sharp declines of most of the 12 curves in particular calendar months, thus ENSO has the spring barrier: the correlations drop below the 95% confidence level in April–June for most of the 12 curves. To effectively detect the spatial extent and timing of the persistence barrier of SSTAs in the tropical Pacific and North Pacific (20°S–70°N), lag correlation was analyzed at each space grid for all 12 starting months. For each space grid, spring persistence barrier was recognized if most of the 12 correlation curves (>10) dropped below 95% confidence level during the boreal spring (April–June), and summer persistence barrier was recognized if most of the 12 correlation curves dropped below 95% confidence level during the boreal summer (July–September). In this way, we determined the spatial–temporal distribution of the persistence barrier of SSTAs in the tropical Pacific and the North Pacific (Fig. 1).

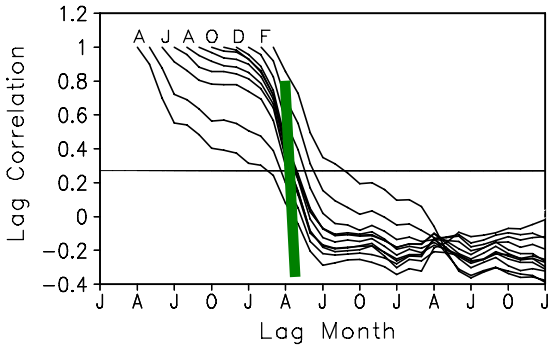

Fig. 2. Lag correlation of SSTAs in the Niño-3 region. Each curve is shifted to line up the starting month (the letters at the start of each curve) with the corresponding lag month (abscissa). The horizontal line indicates the 95% confidence level. Green bar indicates the persistence barrier occurs during spring.

3. Spatial–temporal characteristics of the persistence barrier of SSTAs in the North Pacific

Figure 1a shows the spatial–temporal distribution of the persistence barrier of SSTAs in the tropical Pacific and North Pacific, from IERSST SST data. Clearly, a summer persistence barrier occurs in the SSTAs near 40°N in the CWNP, in addition to the spring persistence barrier in the east equatorial Pacific (mainly in the Niño-3 region). This result indicates that SSTAs persistence in the CWNP significantly decreases in the summer regardless of the starting month and that SSTAs persistence in the east equatorial Pacific significantly decreases in the spring. We sought to verify the result shown in Fig. 1a using HADISST data (Fig. 1b). The two datasets show the persistence barrier in the North Pacific with consistent spatial–temporal characteristics. This agreement suggests that the result is creditable; consequently, IERSST data was used for the following analyses.

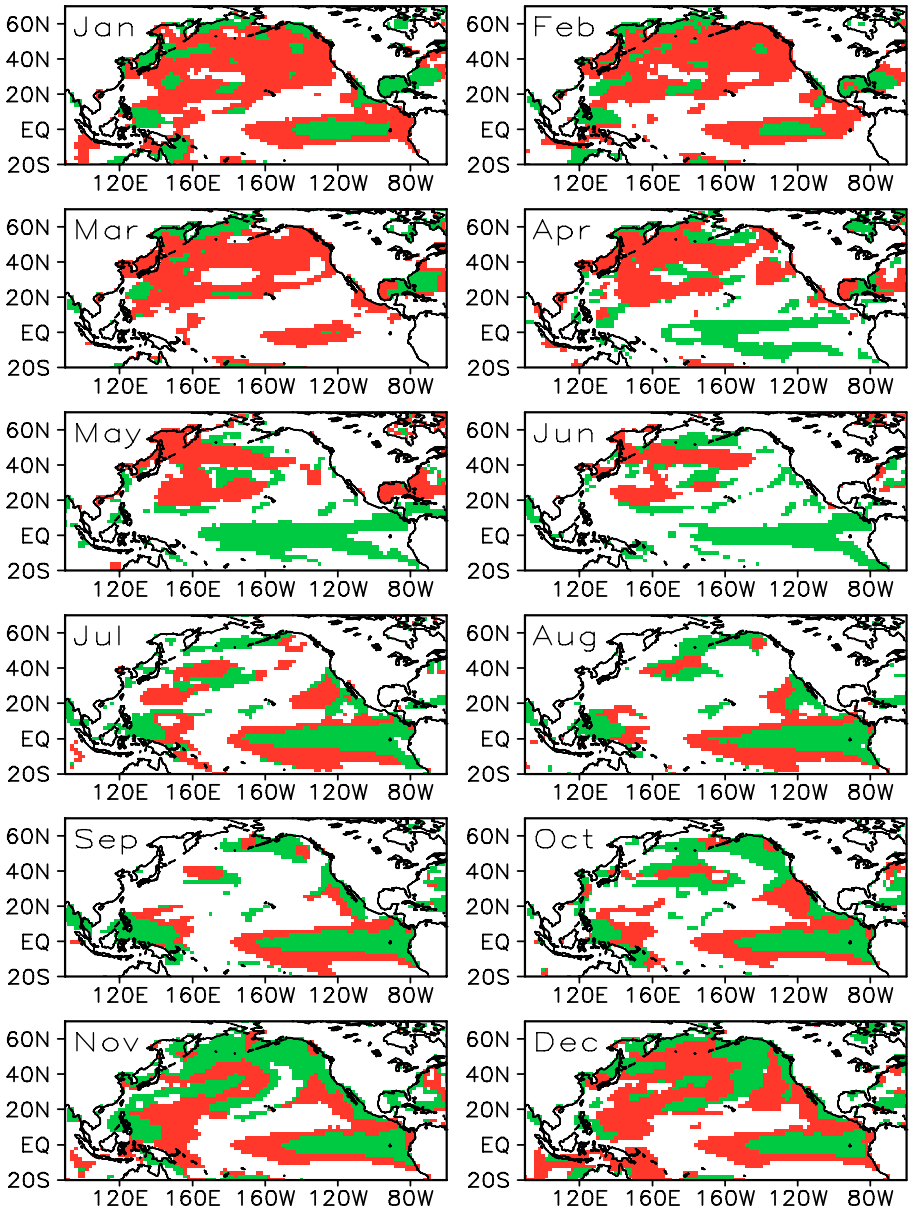

Fig. 3. Seasonal variations in SSTAs persistence in the tropical and North Pacific using IERSST data. For starting months from January to December, green color shading shows the lag correlation of the SSTAs at each grid drops below 95% confidence level in spring; red color shading shows the lag correlation of the SSTAs at each grid drops below 95% confidence levels in summer.

Figure 3 shows the seasonal variation in SSTAs persistence for starting months from January to December. The spatial extent of the spring persistence barrier area in the east equatorial Pacific and the summer persistence barrier area in the North Pacific showed pronounced seasonal change: the former is largest in May and smallest in March, whereas the latter is largest in January–March and smallest in August–September.

To illustrate the behavior of the lag correlation coefficient, we defined the summer persistence barrier region as the CWNP (38°–46°N, 155°E–170°W). For ease of comparison, we also present the result obtained for the Niño-3 region (5°S–5°N, 150°–90°W), where the ENSO spring persistence barrier is mainly located (Fig. 1). Figure 4 shows their lag correlation. The left and right panels show the same information in different forms: the left panels show SSTAs persistence for each starting month, while the right panels show the timing of occurrence of the persistence barrier. For

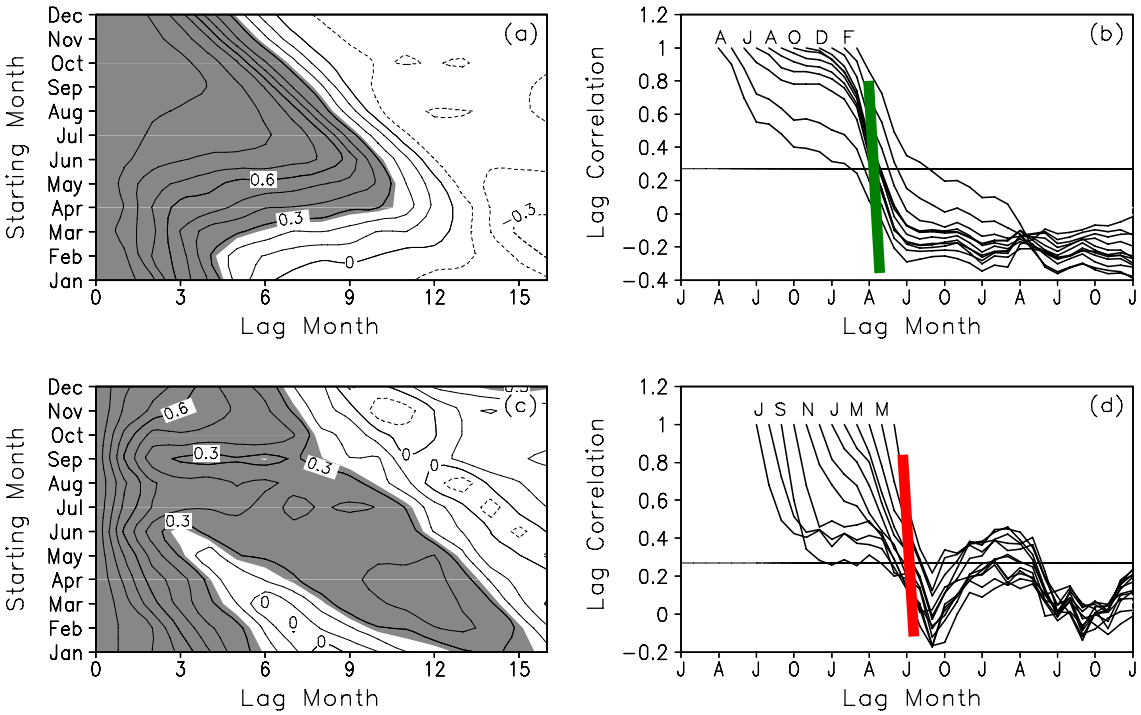

Fig. 4. (a) Lag correlation of SSTAs in the Niño-3 region as a function of starting month (ordinate) and lag month (abscissa) from 1950 to 2004. The contour interval is 0.1 and shading indicates correlation coefficients greater than 95% confidence level. (b) As in panel (a), but viewed as persistence curves as a function of calendar month. Each curve is shifted to line up the starting month (the letters at the start of each curve) with the corresponding lag month (x-axis). The horizontal line indicates the 95% confidence level. (c) As in panel (a), but for SSTAs in the CWNP region. (d) As in panel (b), but for SSTAs in the CWNP region. Green (red) bar indicates the persistence barrier occurs during spring (summer).

the Niño-3 region, the persistence of SSTAs decreases below the 95% confidence level in spring for most of the 12 starting months, indicating that the spring persistence barrier exists in the Niño-3 region (Fig. 4b). SSTAs persistence is longest for starting months of April and May and is shortest for starting months of January and February (Fig. 4a). For the CWNP region, the persistence of SSTAs decreases in summer for most of the 12 starting months, which indicates the existence of the summer persistence barrier (Fig. 4d). SSTAs persistence is longest for starting months of July and August and is shortest for starting months of May and June (Fig. 4c).

Note that the occurrence of the CWNP summer (ENSO spring) persistence barrier does not mean that SSTAs persistence is short for all summertime (springtime) starting months. For the CWNP region, SSTAs persistence is shortest only for early summer, while SSTAs persistence is the longest for starting months of July–August showing a decrease below the 95% confidence level in the following summer. For the Niño-3 region, SSTAs persistence is shortest only for early spring, while SSTAs persistence is the longest for starting months of April–May showing a decrease below the 95% confidence level in the following spring. In fact, the above characteristics are also evident in previous studies of the ENSO spring persistence barrier (Webster and Yang, 1992) and SCS autumn persistence barrier (Chen et al., 2007; Zhao and Li, 2009).

4. Possible causes of the CWNP summer persistence barrier

4.1 *Phase locking and the persistence barrier*

Previous studies have suggested that the phase locking of ENSO to the annual cycle causes the spring persistence barrier, because ENSO tends to transit from one state to another in spring and because ENSO's variance is the lowest during spring (Webster and Yang, 1992; Torrence and Webster, 1998). As shown in Fig. 5, Niño-3 SST is warmest in spring (Fig. 5a), when its standard deviation is the smallest (Fig. 5b). However, SST in the CWNP shows a maximum during August–September and a minimum during February–April (Fig. 5c), with the standard

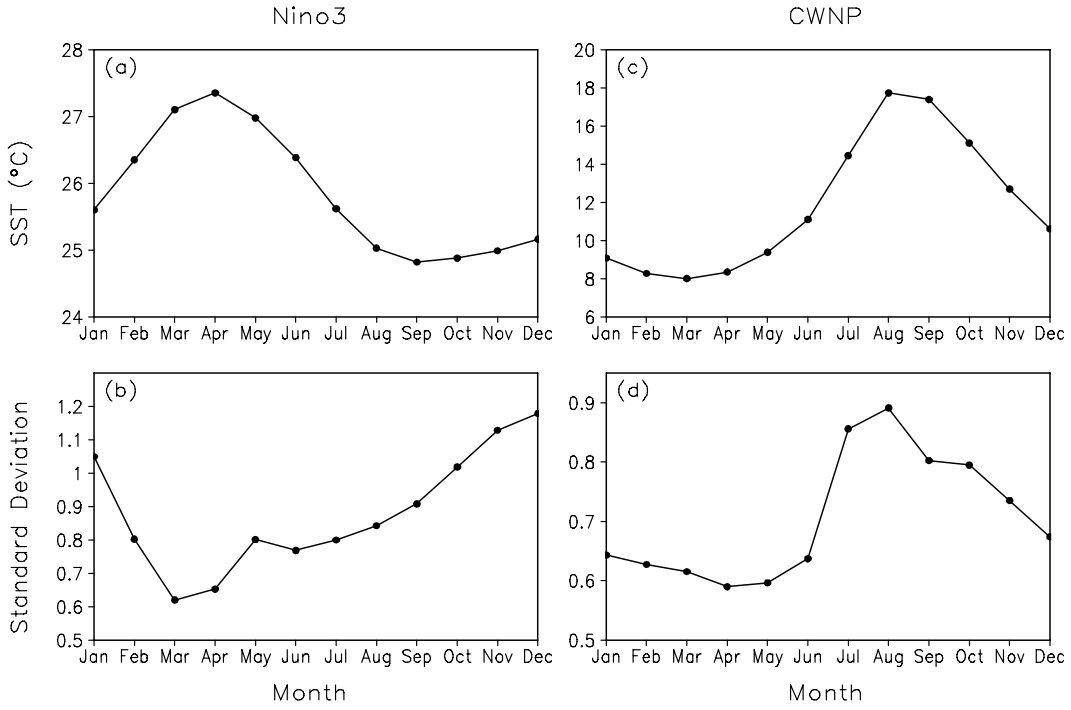

Fig. 5. Annual cycle of SST (upper panels) and standard deviation (bottom panels) for the Niño-3 region (left panels) and the CWNP region (right panels) as a function of calendar month.

deviation showing the same pattern (Fig. 5d). This result indicates that SST and its standard deviation in the CWNP are phase locked to the annual cycle; however, the summer persistence barrier occurs during the maximum phase of the annual cycle of the SST standard deviation. This seasonal contrast of SST variability in the CNWP region is consistent with the mixed-layer depth, which is shallow in summer and deep in winter, suggesting that even a small atmosphere–ocean surface anomaly can induce large SST change (Kara et al., 2003; Wu and Kinter, 2010). Therefore, for the relationship between persistence barrier and phase locking to the annual cycle, the CWNP summer persistence barrier is substantially different from the ENSO spring persistence barrier.

4.2 *Mean seasonal cycle of mixed layer depth and the summer persistence barrier*

A simple stochastic climate model for mid-latitude SST variability, assuming that ocean mixed-layer temperature anomalies (equivalent to SSTAs) are forced by random atmospheric variability and decay by damping back to the atmosphere (Frankignoul and Hasselmann, 1977), provides a good first-order representation of the statistical properties of SSTAs in mid-latitude regions (Frankignoul, 1985). The governing equation for the simple stochastic climate model is

$$\rho c_p h \frac{dT'}{dt} = F' - \lambda T' \,, \tag{1}$$

where ρ is the density of seawater, c_p is the heat capacity of seawater, h is the mean maximum mixed layer depth, T' is the mixed layer temperature anomalies, F' represents the atmospheric forcing of T', and λ is a linear damping coefficient. If the stochastic atmospheric forcing of SSTAs is specified to be "white" in time (i.e., the decorrelation time scale for variations in atmospheric weather is much shorter than that for SST fluctuations), SSTAs would decay exponentially at a rate proportional to the inverse of the mean maximum MLD:

$$r(\tau) = \exp[-\lambda\tau/\rho c_p h] \,. \tag{2}$$

Namely, the deeper the mixed layer, the greater the associated thermal inertia, which is manifested as a longer persistence time. This model yields typical e-folding time scales for SSTAs on the order of 3–6 months, depending on the value used for mixed-layer depth (e.g., Deser et al., 2003).

Figure 6 shows the climatological MLD in the North Pacific for winter (February) and summer (July), and the differences between the two seasons.

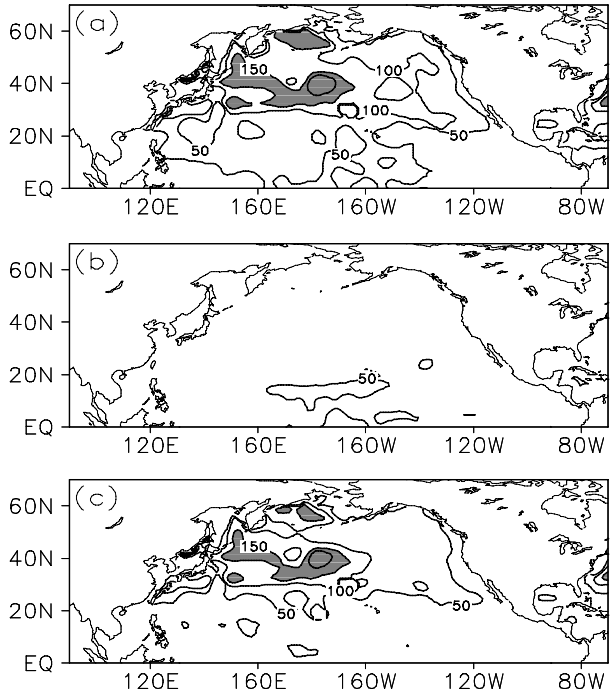

Fig. 6. Climatological mixed layer depth (MLD) in the North Pacific in February (a) and July (b). (c) Climatological MLD differences between February and July; shading indicates a difference >150 m.

The MLD in the North Pacific is deeper in winter (Fig. 6a) and shallower (30 m) in summer (Fig. 6b). The spatial distribution of the difference in the climatological MLD between February and July in the Northern Hemisphere (Fig. 6c) is basically consistent with the distribution of the maximum MLD in February (Fig. 6a). The seasonal variation in the MLD is greatest within the CWNP region.

Based on the simple stochastic climate model in Eq. (1), it might be tempting to conclude that SSTAs persistence in the CWNP is much shorter in summer and longer in winter from Eq. (2). However, this model cannot explain the longest SSTAs persistence starting from summer (July–August) of SSTAs in the CWNP. This shortcoming arises because the model assumes that SSTAs are forced by random atmospheric variability and decay by damping back to the atmosphere; consequently, the modeled atmospheric forcing has a short decorrelation time scale (a week or two) with a white-noise power spectrum at lower frequencies (Frankignoul and Hasselmann, 1977), and SSTAs are not influenced by dynamical processes in the ocean interior. Therefore, both ocean dynamical processes and atmospheric forcing should be considered as physical processes contributing to the summer persistence barrier in the CWNP.

4.3 *Local ocean process and atmospheric forcing*

4.3.1 *Persistence starting in wintertime and the summer persistence barrier*

One important feature of the summer persistence barrier is the significant summertime decline in wintertime SSTAs persistence in the CWNP. Figure 7a shows the lag correlation between SSTAs in February and monthly SSTAs from February of the current year through February of the year after next. SSTAs in the CWNP tend to recur from one winter to the next, without persisting through the intervening summer (Fig. 7a). This seasonal difference in the persistence of SSTAs is closely tied to upper ocean processes (Namias and Born, 1970, 1974; Alexander and Deser, 1995; Zhao and Li, 2010; Zhao and Li, 2012). Figure 7b shows the lag correlation between SSTAs with subsurface temperature anomalies from the surface down to 400 m. Temperature perturbations extend down to the base of the deep winter mixed layer, then the winter thermal anomalies become sequestered beneath the shallow summer mixed layer (Fig. 7b). In this way, the wintertime SSTAs do not persist through the intervening summer. Geographical location of the CWNP region is consistent with the "Region n-NP (37°–45°N, 157°E–179°W)" detected by Hanawa and Sugimoto (2004). They also have indicated that, in Regions n-NP, the anomalous water formed in the winter deepest mixed layer is capped by the shallow seasonal thermocline during the warming season, then subsurface water is entrained due to the mixed layer deepening during the next cooling season.

This ocean process is not the only factor that influences wintertime SSTAs persistence in the CWNP: there may be multiple paths by which wintertime SSTAs decay significantly in summer and recur in the following winter, for example, forcing of atmospheric circulation anomalies at mid–high latitudes in the North Pacific. Zhao and Li (2010) reported that atmospheric circulation anomalies in the North Pacific show winter recurrence without persisting through the intervening summer (their Fig. 6), which is essential for SSTAs persistence in the North Pacific (their Fig. 9).

4.3.2 *Persistence starting in summertime and the summer persistence barrier*

Another important feature of the summer persistence barrier is that SSTAs persistence in the CWNP is longest for the starting month of summer (July), showing a significant decline in the following summer (Fig. 7c). Persistence of summer temperature after February (Fig. 7d) is similar with that of winter SSTAs (Fig. 7b): the summertime temperature anomaly ap-

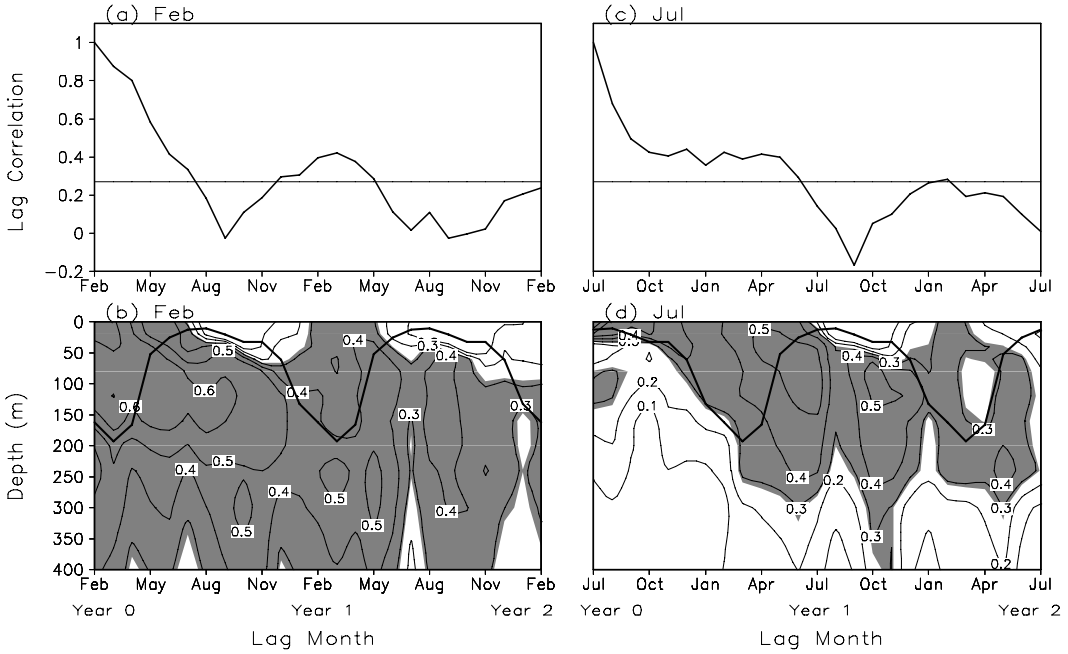

Fig. 7. (a) Lag correlation between SSTAs in the starting month of February and monthly SSTAs from February of the current year (Year 0) through February of the year after the following (Year 2) in the CWNP region from 1955 to 2003. The horizontal line indicates the 95% confidence level. (b) Lag correlations between SSTAs in the CWNP for a starting month of February and temperature anomalies between the surface and 400 m from the current February through February of the year after next. (c) and (d) As in panels (a) and (b), but for a starting month of July. The contour interval is 0.1 and the shaded region indicates statistical confidence above the 95% level. The climatological MLD is shown by the thick line.

pears in deeper ocean layers during the following winter–spring (Year 0 to Year 1), and then becomes sequestered beneath the shallow summer mixed layer during the second summer (Year 1). There is a distinct difference in SSTAs persistence between summer and winter. Winter SSTAs do not persist through the intervening summer (Fig. 7b). But summer SSTAs could persist above 50 m during July–November of Year 0 (Fig. 7d), demonstrating decoupling of the shallow summertime mixed layer from the temperature anomalies below the base of the mixed layer. Therefore, some positive feedback processes must operate at the atmosphere–ocean interface to induce summertime SSTAs and prolong their persistence.

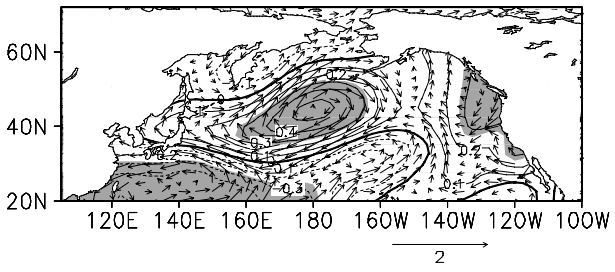

Fig. 8. Correlation between SSTAs in the CWNP region and geopotential height (contour) and wind (vector) anomalies at 850 hPa in the North Pacific during summer (July). The counter interval is 0.1, and shading indicates correlation coefficient values with 95% confidence level.

Figure 8 shows correlation between SSTAs in the CWNP region and geopotential height (GPH) and wind anomalies at 850 hPa in the North Pacific during summer (July). There are significantly positive correlations between the atmospheric circulation anomalies and SSTAs during summer. And this positive SST–GPH correlation is accompanied by an anomalous anticyclone during summer over the North Pacific. There is a coincidence between pressure patterns from lower troposphere to upper troposphere, because the summertime atmospheric filed generally has a quasi-barotropic structure (Fig. 9). Positive (negative) GPH anomalies with anomalous easterlies (westerlies) are associated with an anomalous anticyclone (cyclone) over warm (cool) SSTAs (e.g., Wu and Kinter, 2010). This positive SST-GPH correlation is indicative of atmosphere forcing to ocean (e.g., An and Wang, 2005; Wu and Kinter, 2010). Therefore, it appears that atmospheric circulation anomalies also play an important role in sustaining SSTAs starting in summertime in the CWNP region, although the influence of atmos-

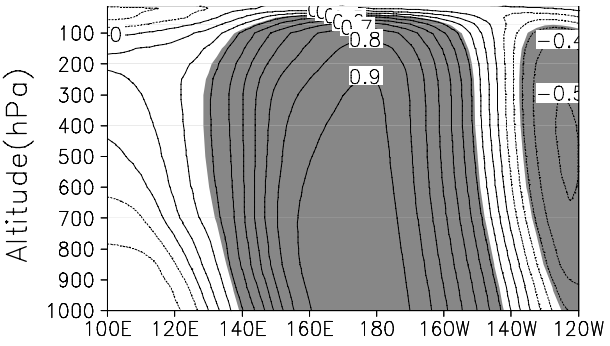

Fig. 9. Correlation between SLP anomalies in the CWNP region and geopotential height anomalies from 1000 hPa to 70 hPa along 40°N during summer (July). The shaded region indicates statistical confidence above the 95% level.

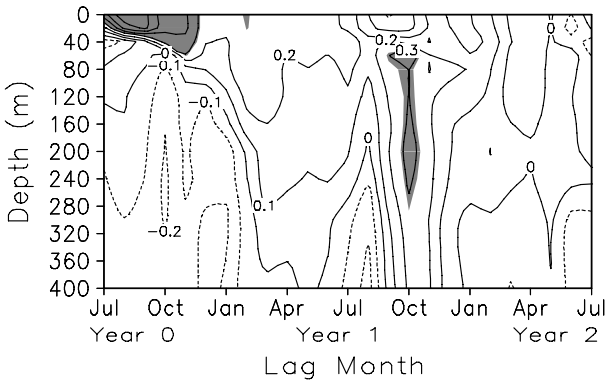

Fig. 10. Lag correlations between geopotential height anomalies at 850 hPa in the CWNP for a starting month of July and oceanic temperature anomalies between the surface and 400 m from the current July through July of the year after next from 1955 to 2003. The contour interval is 0.1 and the shaded region indicates statistical confidence above the 95% level.

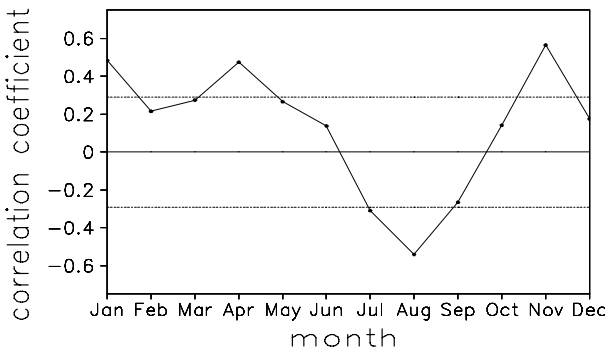

Fig. 11. Correlation between SSTAs in the CWNP region and low cloud cover anomalies for each calendar month from 1958 to 2001. The thin solid line indicates the 95% confidence level.

pheric anomalies on the summer oceanic temperature anomalies is only sustained to November (Fig. 10).

Wu and Kinter (2010) have indicated that, in summertime, a large anomalous anticyclone occupies most of the North Pacific, which can induce anomalous descent and reduce cloudiness; thus it may contribute to the enhancement in the downward shortwave radiation and the original SSTAs. Although the positive cloud feedback on SSTAs to prolong the summertime SSTAs persistence in the North Pacific was first mentioned by Zhang et al. (1998), they did not investigate in detail the role of cloud–SSTAs interactions in sustaining the summertime SSTAs. Figure 11 shows the simultaneous correlation between SSTAs and low cloud cover anomalies in the CWNP for each calendar month, which shows the seasons for which the ocean and low cloud are highly correlated. Obviously, low-cloud anomalies are negatively correlated with SSTAs during July–September, suggesting a positive cloud feedback on SSTAs over the CWNP (Norris et al., 1998). However, this positive feedback is not sustained for long, because their correlations become positive after October. Thus, the positive cloud feedback plays an important role during summertime over the North Pacific, but it only works during the initial stage of the summertime SSTAs persistence in the CWNP.

4.4 *Remote ENSO forcing*

As the leading mode of interannual variability in the climate system, ENSO has a strong influence on climate variability in the North Pacific. It is interesting to consider whether ENSO influences the CWNP summer persistence barrier. Figure 12a shows the lead–lag correlation between SSTAs in CWNP and the Niño-3 region. The strongest negative correlations occur when SSTAs in the Niño-3 region lead those in the CWNP by 3–4 months. It appears that the occurrence of the CWNP summer persistence barrier is linked to the spring persistence barrier in the Niño-3 region, because the timing of the spring persistence barrier in the Niño-3 region is earlier (by one season) than that of the summer persistence barrier in the CWNP. However, many studies have reported an intrinsic mid-latitude atmosphere–ocean coupled mode in the North Pacific (e.g., Zhang et al., 1996, 1997; An and Wang, 2005), for which SSTAs are mainly confined to the extratropical North Pacific with the maximum loading of the dominant pattern located in the CWNP region, and atmospheric variation leads to changes in SST, in contrast to the case for the ENSO mode.

To further consider the influence of ENSO on the CWNP summer persistence barrier, we performed a linear regression analysis. SSTAs variability associated

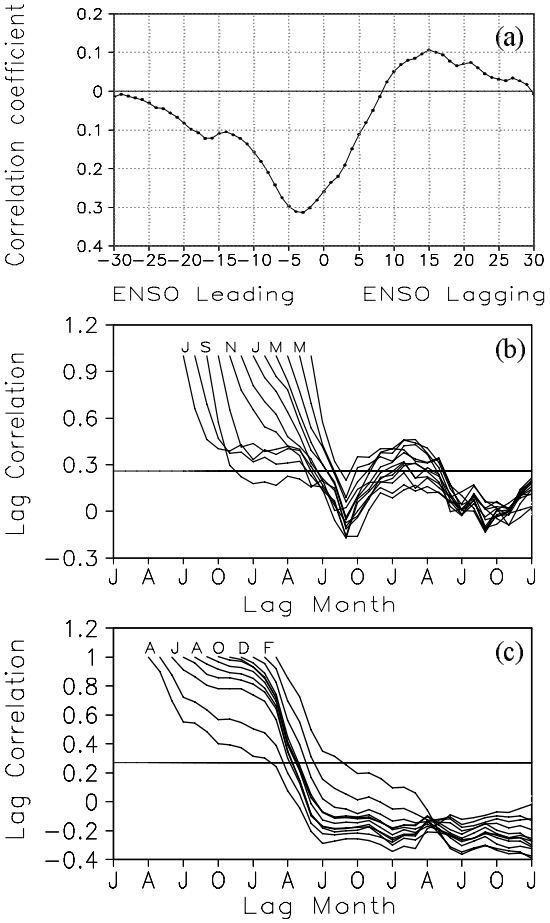

Fig. 12. (a) Monthly lead–lag correlation between SSTAs in the CWNP region and the Niño-3 region. Negative lags refer to SSTAs in the Niño-3 region leading those in CWNP. (b) Lag correlation of SSTAs in the CWNP region, but with the ENSO-regressed SSTAs subtracted from the original data. (c) Same as panel (b), but for the ENSO-regressed SSTAs.

with the ENSO cycle is obtained by regressing SSTAs in the CWNP upon the simultaneous SSTAs in the Niño-3 region. This regression value was subtracted from the original SSTAs in the CWNP to yield the residual SSTAs excluding ENSO-related variability in SST. From the variance analysis, the ratio of the ENSO-regressed variance to the total variance of SSTAs in the CWNP region was only ∼8%, while the ratio was ∼92% for the CWNP SSTAs without the ENSO signal. Due to the persistence characteristics of ENSO itself, the ENSO-regressed CWNP SSTAs also exhibited spring persistence barrier (Fig. 12c). But the CWNP SSTAs without the ENSO signal exhibited summer persistence barrier (Fig. 12b) similar to that in the original SSTAs data (Fig. 4d). This similarity was retained by regressing CWNP SSTAs upon Niño-3 SSTAs for a 3–4-month lead time, which showed their strongest correlation (Fig. 12a). These analyses focused on the Niño-3 region where the ENSO spring persistence barrier is mainly located (Fig. 1). We further expanded our analysis to three other ENSO regions (i.e., the Niño-1+2, Niño-3.4, and Niño-4 regions), to determine whether remote ENSO variability has little linear influence on the occurrence of the summer persistence barrier of SSTAs in the CWNP, because ENSO events show different characteristics in terms of location of maximum SSTAs compared to conventional El Niño events (Ashok et al., 2007; Kao and Yu, 2009; Kug et al., 2009, and Yeh et al., 2009). The result does not depend on the position of the selected ENSO region (not shown). Above results indicate that remote ENSO variability has little linear influence on the summer persistence barrier of SSTAs in the CWNP. The summer persistence barrier is an inherent persistence characteristic of the SSTAs in the CWNP.

This result is consistent with the observation analysis of An and Wang (2005). They separated the intrinsic mid-latitude atmosphere–ocean coupled mode in the North Pacific (the NP mode) from the ENSO-induced mid-latitude coupled pattern. For the NP mode, atmospheric variation leads to changes in SST, and the NP mode displays a persistence barrier during summer. However, in model simulations, the impact of remote ENSO forcing on SSTAs persistence in North Pacific remains uncertain. On one hand, ENSO events are not essential for SSTAs persistence in the North Pacific in wintertime, although SSTAs in the tropical Pacific associated with ENSO affect the wintertime SST in the North Pacific via changes in the extratropical atmospheric circulation, as shown by coupled atmosphere–ocean model simulations (Alexander and Scott, 2001). On the other hand, although the magnitude of ENSO-related forcing is much smaller than stochastic forcing, the former should still have a strong influence on SSTAs persistence in the central western Pacific region (Park et al., 2006). Using a stochastically forced ocean mixed layer model and an AGCM coupled to a variable-depth mixed layer ocean model, they concluded that ENSO-induced forcing tends to reduce the persistence of winter–spring SSTAs for lags terminating in September, but it enhances autocorrelations for the reference period of August–October, especially for lags of 2–9 months. Overall, causes of this controversy in model simulations are not clear at this stage.

It is well known that both the mid-latitude North Pacific and the east-central tropical Pacific exhibit variations on decadal time scales, with a significant interdecadal climatic regime shift occurring before and after the late 1970s (Trenberth and Shea, 1987; Miller

and Schneider, 2000; An and Wang, 2000; Xiao and Li, 2007; Xiao et al., 2011). Furthermore, recent studies indicate that anomalous warm SST in the central equatorial Pacific has been observed more frequently during recent decades (Ashok et al., 2007; Yeh et al., 2009; Kao and Yu, 2009; Yu et al., 2011). Figure 13 gives the lag correlations of SSTAs in the CWNP for 1950–1975 and 1979–2004, and for which the Niño-1+2, Niño-3, Niño-3.4 and Niño-4 SSTAs have been subtracted, to determine whether the massive averaging (1950–2004) might have destroyed important information of ENSO on the summer persistence barrier in the CWNP. It can be seen that, regardless of which period (before and after the late 1970s), remote ENSO variability has little linear influence on the summer persistence barrier of SSTAs in the CWNP.

4.5 *PDO*

The leading mode of SSTAs in the North Pacific is usually called the Pacific Decadal Oscillation (PDO) (Mantua et al., 1997). The CWNP is located in the center of PDO. What is the difference and relation of persistence between the large SSTAs pattern and local SSTAs? Figure 14 shows the lag correlation of the PDO index. There are similarities and differences in the persistence between the PDO index and the CWNP SSTAs (Figs. 4c and d). On the one hand, their lag correlations starting from July to December exhibit similar characteristics, namely, the SSTAs could persist until the following summer. On the other hand, different persistence characteristics are evident for those with starting months from January to June. The PDO could persist through the summertime except in the starting month of January; while SSTAs in the CWNP recur from one winter to the next without persisting through the intervening summer. It seems that their differences in the SSTAs persistence are mainly for the starting month of the second half of the year. Zhang et al. (1998) also indicated that the dominant pattern of SSTAs exhibits generally higher autocorrelation than the local SSTAs, and the difference is particularly evident in the second half of the calendar year.

To investigate the relationship of persistence between the large SSTAs pattern PDO and local CWNP SSTAs, linear regression was used. Figure 15 shows the lag correlation of SSTAs in the CWNP, in which the PDO-related SSTAs have been subtracted from the local SSTAs in the CWNP. Significant differences in the local SSTAs persistence in the CWNP can be seen, especially for the starting months from July to October, because SSTAs persistence clearly becomes shorter compared with the original result (Fig. 4c). This result suggests that the influence of the PDO on persistence of the CWNP SSTAs is most significant in the late summer to early autumn.

5. Conclusions and discussion

In this study, we examined the persistence barrier of SSTAs in the North Pacific and compared them with the ENSO spring persistence barrier. The results indicate that SSTAs persistence in the CWNP has a remarkable seasonal variation and shows a persistence barrier in summer. Persistence shows a marked drop in summer for the most of the 12 starting months. Note that the occurrence of a summer persistence barrier in the CWNP does not mean that SSTAs persistence is short for all starting months from summertime. For the CWNP, SSTAs persistence is shortest only for early summer, while it is longest for starting months in July–August, showing a significant decline in the following summer. Similarly, the occurrence of a spring persistence barrier in the Niño-3 region does not mean that SSTAs persistence is short for all starting months from springtime. For the Niño-3 region, SSTAs persistence is shortest only for early spring, while it is longest for starting months in April–May, showing a significant decline in the following spring. Compared with the ENSO spring persistence barrier, the spatial distribution of summer persistence barrier in the North Pacific is narrower (Fig. 1). And summer persistence barrier in the CWNP is weaker than spring persistence barrier in the Niño-3 (Fig. 4).

SSTAs variations in the CWNP are phase locked to the annual cycle, whereas the summer persistence barrier occurs during the maximum phase of the annual cycle of SST variance. The ENSO spring persistence barrier occurs during the minimum phase of the annual cycle of ENSO variance. Therefore, for the relationship between persistence barrier and phase locking to the annual cycle, the CWNP summer persistence barrier is substantially different from the ENSO spring persistence barrier.

Further analyses indicate that remote ENSO forcing has little linear influence on the CWNP summer persistence barrier, compared with local upper-ocean processes and atmospheric forcing in the North Pacific. In winter, local ocean processes and atmospheric forcing are both at work in the CWNP. In summer, local atmospheric forcing may be more important because subsurface ocean temperature anomalies do not provide the exclusive source of SSTAs memory starting in summertime. Starting in wintertime, SSTAs extend down to the deep winter mixed layer then become sequestered beneath the shallow summer mixed layer, which is decoupled from the surface layer. Thus, wintertime SSTAs do not persist

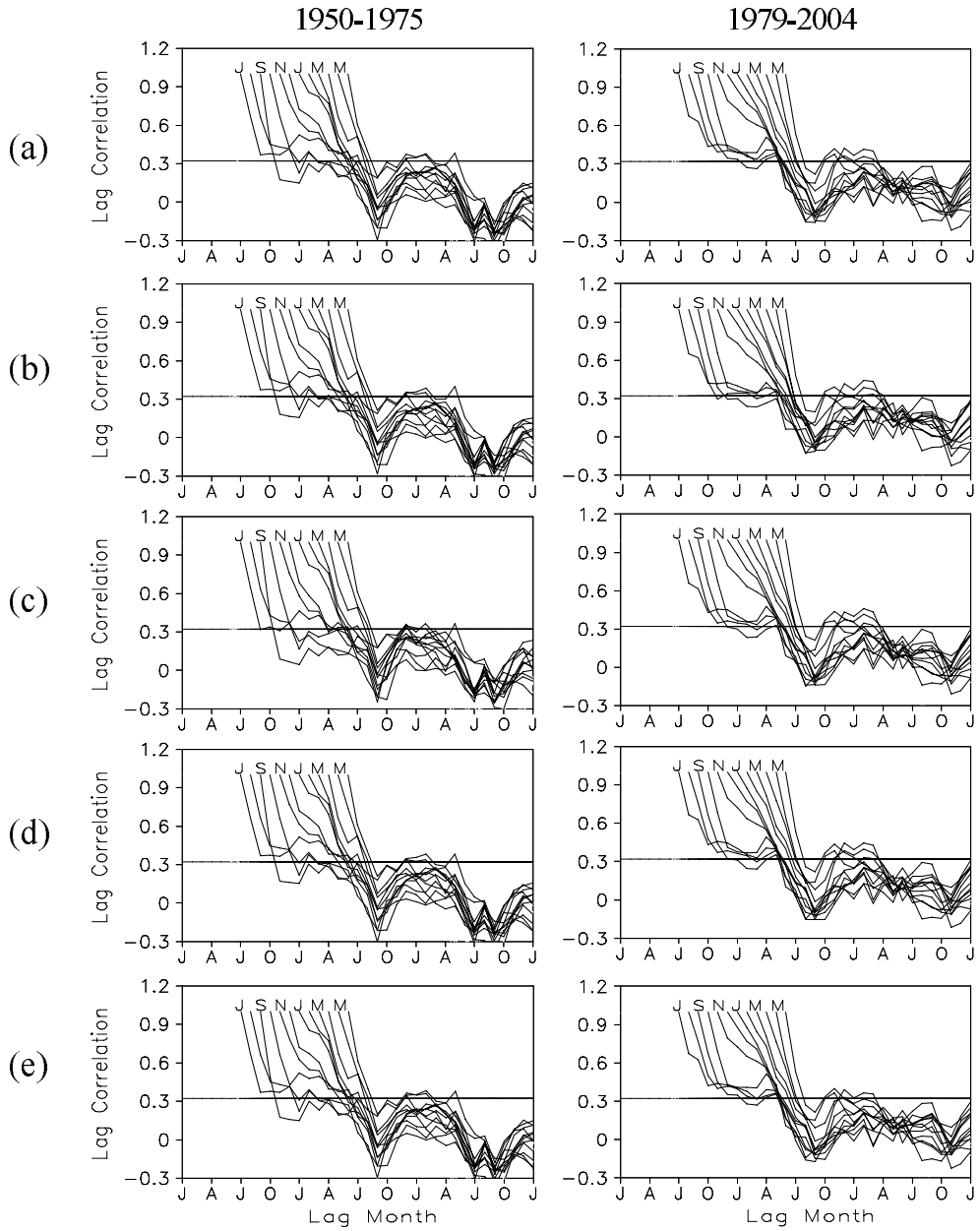

Fig. 13. (a) Lag correlation of SSTAs in the CWNP region for 1950–1975 (left panels) and 1979–2004 (right panels). (b)–(e) As in panel (a), but for which the (b) Niño-1+2, (c) Niño-3, (d) Niño-3.4, and (e) Niño-4 SSTAs have been subtracted, respectively.

through the following summer. Starting in summertime, the shallow summertime mixed layer is decoupled from the temperature anomalies at depth. The persistence of summer SSTAs until autumn can be explained by the atmospheric forcing through a positive SSTAs–cloud/radiation feedback. The following autumn–winter–spring SSTAs persistence is similar to the winter SSTAs persistence when the mixed layer deepens again. Thus, summer SSTAs in the CWNP have a long persistence showing a significant decline in the following summer. In this way, SSTAs in the CWNP have a persistence barrier in summer regardless of the starting month.

Why the summer persistence barrier of SSTAs is only observed in the CWNP region remains an open question. In fact, the CWNP region is unique in several ways: (1) it is located in the key area of the SSTAs variability in the North Pacific (Wu and Kinter, 2010); (2) it is located where the MLD seasonal variation between summer and winter is greatest (Fig. 6c); and (3)

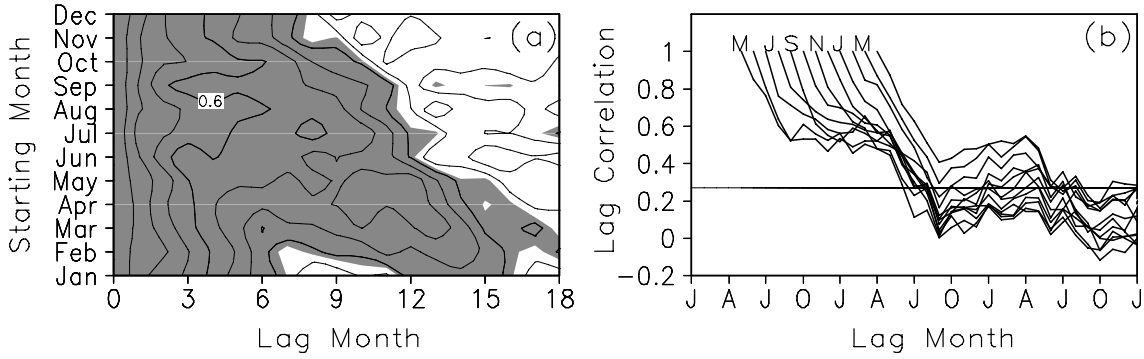

Fig. 14. Lag correlation of the PDO index.

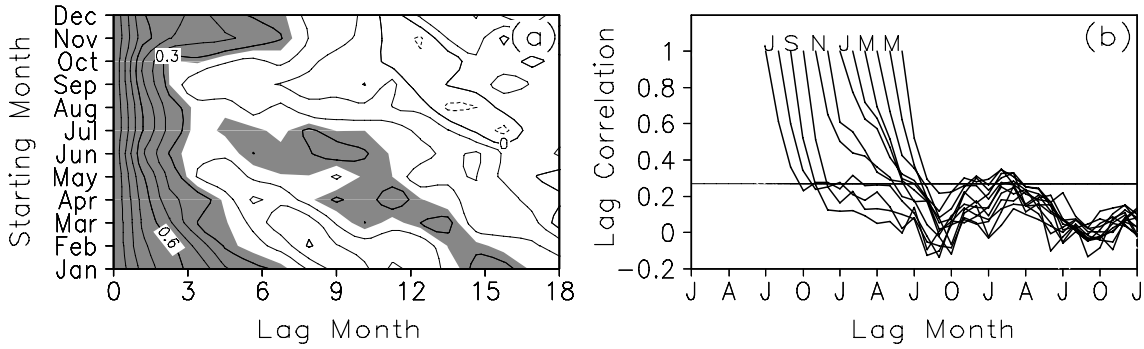

Fig. 15. Same as Figs. 4c and d, but the PDO-related SSTAs have been subtracted from the original SSTAs in the CWNP.

it is located where the shortwave radiation change associated with a positive cloud–SST feedback is a dominant factor for the development of SSTAs in boreal summer (Norris et al., 1998; Wu and Kinter, 2010). Whether these particularities cause the CNWP region to be the only persistence barrier region in the North Pacific is unclear and remains to be further studied.

Acknowledgements. This work was jointly supported by the 973 program (Grant No. 2010CB950400), the Innovation Key Program (Grant No. KZCX2-YW-Q11-02) of the Chinese Academy of Sciences, the NSFC project (Grant Nos. 41030961, 41005042, and 41005049), the Fund of State Key Laboratory of Tropical Oceanography (South China Sea Institute of Oceanology, Chinese Academy of Sciences (LTO1101), and the 973 program (Grant No. 2012CB956000).

REFERENCES

Alexander, M. A., and C. Deser, 1995: A mechanism for the recurrence of wintertime midlatitude SST anomalies. *J. Phys. Oceanogr.*, **25**, 122–137.

Alexander, M. A., and J. D. Scott, 2001: Winter-to-winter recurrence of sea surface temperature, salinity and mixed layer depth anomalies. *Prog. Oceanogr.*, **49**, 41–61.

An, S.-I., and B. Wang, 2000: Interdecadal change of the structure of the ENSO mode and its impact on the ENSO frequency. *J. Climate,* **13**, 2044–2055.

An, S. I., and B. Wang, 2005: The forced and intrinsic low-frequency modes in the North Pacific. *J. Climate,* **18**, 876–885.

Ashok, K., S. K. Behera, S. A. Rao, H. Weng, and T. Yamagata, 2007: El Niño Modoki and its possible teleconnection. *J. Geophys. Res.,* **112**(C11007), doi: 10.1029/2006JC003798.

Cayan, D. R., 1992: Latent and sensible heat flux anomalies over the northern oceans: Driving the sea surface temperature. *J. Phys. Oceanogr.,* **22**, 859–881.

Chen, J. M., T. Li, and C. F. Shih, 2007: Fall persistence barrier of sea surface temperature in the South China Sea associated with ENSO. *J. Climate,* **20**, 158–172.

Clarke, A. J., and S. van Gorder, 1999: The connection between the boreal spring Southern Oscillation PB and biennial variability. *J. Climate,* **12**, 610–620.

Davis, R. E., 1978: Predictability of sea level pressure anomalies over the North Pacific Ocean. *J. Phys. Oceanogr.*, **8**, 233–246.

Deser, C., and M. L. Blackmon, 1995: On the relationship between tropical and North Pacific sea surface temperature variations. *J. Climate,* **8**, 1677–1680.

Deser, C., M. A. Alexander, and M. S. Timlin, 2003: Understanding the persistence of sea surface tempera-

ture anomalies in midlatitudes. *J. Climate,* **16**, 57–72.

Ding, R., and J. Li, 2009: Decadal and seasonal dependence of North Pacific sea surface temperature persistence. *J. Geophys. Res.*, **114**(D01105), doi: 10.1029/2008JD010723.

Ding, R., and J. Li, 2011: Winter persistence barrier of sea surface temperature in the northern tropical Atlantic associated with ENSO. *J. Climate*, **24**, doi: 10.1175/2011JCLI3784.1.

Duan, W. S., and R. Zhang, 2010: Is model parameter error related to a significant spring predictability barrier for El Niño events? Results from a theoretical model. *Adv. Atmos. Sci.*, **27**, 1003–1013, doi: 10.1007/s00376-009-9166-4.

Duan, W. S., X. Liu, K. Y. Zhu, and M. Mu, 2009: Exploring initial errors that cause a significant spring predictability barrier for El Niño events. *J. Geophys. Res.,* **114**(C04022), doi: 10.1029/2008JC004925.

Frankignoul, C., 1985: Sea surface temperature anomalies, planetary waves and air-sea feedback in middle latitudes. *Rev. Geophys.*, **23**, 357–390.

Frankignoul, C., and K. Hasselmann, 1977: Stochastic climate models. Part 2. Application to sea-surface temperature variability and thermocline variability. *Tellus*, **29**, 289–305.

Hanawa, K., and S. Sugimoto, 2004: "Reemergence" areas of winter sea surface temperature anomalies in the world's oceans. *Geophys. Res. Lett.*, **31**, L10303, doi: 10.1029/2004GL019904.

Kalnay, E., and Coauthors, 1996: The NCEP/ NCAR 40-year reanalysis project. *Bull. Amer. Meteor. Soc.*, **77**, 437–471.

Kao, H.-Y., and J. Y. Yu, 2009: Contrasting eastern-Pacific and Central-Pacific types of El Niño. *J. Climate*, **22**, 615–632.

Kara, A. B., P. A. Rochford, and H. E. Hurlburt, 2003: Mixed layer depth variability over the global ocean. *J. Geophys. Res.*, **108**(C3), 3079, doi: 10.1029/2000JC000736.

Kug, J. S., F. F. Jin, and S. I. An, 2009: Two types of El Niño events: Cold tongue El Niño and warm pool El Niño. *J. Climate*, **22**, 1499–1515.

Kushnir, Y., and N.-C. Lau, 1992: The general circulation model response to a North Pacific SST anomaly: Dependence on time scale and pattern polarity. *J. Climate,* **5**, 271–283.

Lau, K. M., and S. Yang, 1996: The Asian monsoon and predictability of the tropical ocean-atmosphere system. *Quart. J. Roy. Meteor. Soc.*, **122**, 945–957.

Lau, N. C., and M. J. Nath, 1990: A general circulation model study of the atmospheric response to extratropical SST anomalies observed in 1950–79. *J. Climate,* **3**, 965–989.

Lau, N. C., and M. J. Nath, 1996: The role of the "atmospheric bridge" in linking tropical Pacific ENSO events to extratropical SST anomalies. *J. Climate,* **9**, 2036–2057.

Mantua, J. N., S. R. Hare, Y. Zhang, J. M. Wallace, and R. C. Francis, 1997: A Pacific interdecadal climate oscillation with impacts on salmon production. *Bull. Am. Meteorol. Soc.*, **78**, 1069–1079, doi: 10.1175/1520-0477(1997)078<1069:APICOW>2.0.CO;2

Miller, A. J., and N. Schneider, 2000: Interdecadal climate regime dynamics in the North Pacific Ocean: Theories, observations and ecosystem impacts. *Prog. Oceanogr.*, **47**, 257–260.

Monterey, G. I., and S. Levitus, 1997: Seasonal variability of mixed layer depth for the world ocean. NOAA Atlas NESDIS 14, US Gov. Printing Office, Washington, DC., 92pp.

Mu, M., H. Xu, and W. S. Duan, 2007: A kind of initial errors related to "spring predictability barrier" for El Niño events in Zebiak-Cane Model. *Geophys. Res. Lett.*, **34**(L03709), doi: 10.1029/2006GL-27412.

Namias, J., and R. M. Born, 1970: Temporal coherence in North Pacific sea-surface temperature patterns. *J. Geophys. Res.*, **75**, 5952–5955.

Namias, J., and R. M. Born, 1974: Further studies of temporal coherence in North Pacific sea surface temperatures. *J. Geophys. Res.*, **79**, 797–798.

Norris, J. R., Y. Zhang, and J. M. Wallace, 1998: Role of clouds in summertime atmosphere-ocean interactions over the North Pacific. *J. Climate,* **11**, 2482–2490.

Pan, Y. H., and A. H. Oort, 1990: Correlation analyses between sea surface temperature anomalies in the eastern equatorial Pacific and the World Ocean. *Climate Dyn.*, **4**, 191–205.

Park, S., M. A. Alexander, and C. Deser, 2006: The impact of cloud radiative feedback, remote ENSO forcing, and entrainment on the persistence of North Pacific sea surface temperature anomalies. *J. Climate,* **19**, 6243–6261.

Rayner, N. A., D. E. Parker, E. B. Horton, C. K. Folland, L. V. Alexander, D. P. Rowell, E. C. Kent, and A. Kaplan, 2003: Global analyses of sea surface temperature, sea ice, and night marine air temperature since the late nineteenth century. *J. Geophys. Res.*, **108**(D14), 4407, doi: 10.1029/2002JD002670.

Smith, T. M., and R. W. Reynolds, 2004: Improved extended reconstruction of SST (1854–1997). *J. Climate,* **17**, 2466–2477.

Torrence, C., and P. J. Webster, 1998: The annual cycle of persistence in the El Niño/Southern Oscillation. *Quart. J. Roy. Meteor. Soc.*, **124**, 1985–2004.

Trenberth, K., and D. J. Shea, 1987: On the evolution of the Southern Oscillation. *Mon. Wea. Rev.,* **115**, 3078–3096.

Trenberth, K. E., G. W. Branstator, D. Karoly, A. Kumar, N.-C. Lau, and C. Ropelewski, 1998: Progress during TOGA in understanding and modeling global teleconnections associated with tropical sea surface temperatures. *J. Geophys. Res.,* **103**, 14291–14324.

Troup, A. J., 1965: The "southern oscillation". *Quart. J. Roy. Meteor. Soc.*, **91**, 490–506.

Uppala, S. M., and Coauthors, 2005: The ERA-40 reanalysis. *Quart. J. Roy. Meteor. Soc.*, **612**, 2961–

3012.

Wajsowicz, R. C., 2005: Potential predictability of tropical Indian Ocean SST anomalies. *Geophys. Res. Lett.*, **32**(L24702), doi: 10.1029/2005GL024169.

Wallace, J. M., C. Smith, and Q. Jiang, 1990: Spatial patterns of atmosphere-ocean interaction in the northern winter. *J. Climate*, **3**, 990–998.

Webster, P. J., and S. Yang, 1992: Monsoon and ENSO: Selectively interactive systems. *Quart. J. Roy. Meteor. Soc.*, **118**, 877–925.

White, W. B., 1995: Design of a global observing system for gyrescale upper ocean temperature variability. *Prog. Oceanogr.,* **36**, 169–217.

Wright, P. B., 1979: Persistence of rainfall anomalies in the central Pacific. *Nature*, **277**, 371–374.

Wu, R., and J. L. Kinter, 2010: Atmosphere-ocean relationship in the midlatitude North Pacific: Seasonal dependence and east-west contrast. *J. Geophys. Res.,* **115**, D06101, doi: 10.1029/2009JD012579.

Xiao, D., and J. Li, 2007: Spatial and temporal characteristics of the decadal abrupt changes of global atmosphere-ocean system in the 1970s. *J. Geophys. Res.*, **112(**D24S22), doi: 10.1029/2007JD008956.

Xiao, D., J. Li, and P. Zhao, 2011: Four-dimensional structures and physical process of the decadal abrupt changes of the northern extratropical ocean-atmosphere system in 1980s. *Int. J. Climatol.*, **31**, doi: 10.1002/joc.2326.

Xue, Y., M. A. Cane, S. E. Zebiak, and M. B. Blumenthal, 1994: On the prediction of ENSO: A study with a low-order Markov model. *Tellus*, **46**, 512–528.

Yeh, S.-W., J. S. Kug, B. Dewitte, M. H. Kwon, B. P. Kirtman, and F. F. Jin, 2009: El Niño in a changing climate. *Nature*, **461**, 511–514.

Yu, J. Y., 2005: Enhancement of ENSO's PB by biennial variability in a coupled atmosphere-ocean general circulation model. *Geophys. Res. Lett.*, **32**(L113707), doi: 10.1029/2005GL023406.

Yu, J. Y., H. Y. Kao, T. Lee, and S. T. Kim, 2011: Subsurface ocean temperature indices for central-Pacific and eastern-Pacific types of El Niño and La Niña events. *Theor. Appl. Climatol.*, **103**, 337–344.

Zhang, Y., J. M. Wallace, and N. Iwasaka, 1996: Is climate variability over the North Pacific a linear response to ENSO? *J. Climate*, **9**, 1468–1478.

Zhang, Y., J. M. Wallace, and D. S. Battisti, 1997: ENSO-like interdecadal variability: 1900–93. *J. Climate*, **10**, 1004–1020.

Zhang, Y., J. R. Norris, and J. M. Wallace, 1998: Seasonality of large scale atmosphere-ocean interaction over the North Pacific. *J. Climate,* **11**, 2473–2481.

Zhao, X., and J. Li, 2009: Possible causes for the persistence barrier of SSTA in the South China Sea and the vicinity of Indonesia. *Adv. Atmos. Sci.,* **26**, 1125–1136, doi: 10.1007/s00376-009-8165-9.

Zhao, X., and J. Li, 2010: Winter-to-winter recurrence of SSTA in the Northern Hemisphere. *J. Climate*, **23**, 3835–3854, doi: 10.1175/2009JCLI2583.1.

Zhao, X., and J. Li, 2012: Winter-to-winter recurrence and non-winter-to-winter recurrence of SST anomalies in the central North Pacific. *J. Geophys. Res,* **117**, C05027, doi: 10.1029/2011JC007845.